PHYSICAL REVIEW B

CONDENSED MATTER

THIRD SERIES, VOLUME 39, NUMBER 11 15 APRIL 1989-I

Multiple-scattering approach to oxygen K near-edge structures in electron-energy-loss spectroscopy of alkaline earths

Xudong Weng and Peter Rez

Center of Solid State Science and Department of Physics, Arizona State University, Tempe, Arizona 85287-1704

(Received 3 October 1988)

The multiple-scattering approach to the calculation of fine structure in inner-shell electron-energy-loss spectroscopy is based on a muffin-tin potential approximation. In order to extract information on atomic environment and charge transfer, it is essential to understand the relationship between the near-edge structures and the crystal potential. We compare the oxygen K near-edge structure of MgO, CaO, and SrO calculated with two commonly used ground-state muffin-tin potential models for ionic materials. Although the muffin-tin potential and the phase shifts are quite different, we found that these two models are both capable of yielding near-edge structure which is in reasonable agreement with the experimental spectra. Our results suggest that multiple-scattering calculations may not be able to differentiate between these two models for the muffin-tin potential. It appears that the near-edge structure is more affected by geometry than possible charge transfer.

I. INTRODUCTION

In analytical electron-energy-loss spectroscopy (EELS) in the electron microscope,[1,2] the excitation of inner-shell electrons by the incident electron beam is of particular interest due to the fact that inner-shell loss edges are characteristic of the chemical composition. We can therefore use them to acquire information on both the elemental concentration and the atomic environment. The microanalysis of elemental compositions is now routinely carried out by making use of appropriate cross sections for the microscope accelerating voltage and collection angles used.[3–5] The atomic environment can be studied through both the electron-energy-loss near-edge fine structures (ELNES) (Refs. 6–16) and extended x-ray-edge energy-loss fine structures (EXELFS),[17,18] which are very similar to the corresponding fine structures of x-ray absorption spectroscopy.[19–25] As EELS is sensitive to light elements, ELNES could be used to study compounds of carbon, nitrogen, oxygen, and fluorine. Together with the high spatial resolution in the electron microscope, ELNES can also be used to determine the local bonding and electronic structure across interfaces.[26]

In this paper, we study the oxygen K near-edge structures of selected alkaline earths, MgO, CaO, and SrO, using a real-space Green-function-type multiple-scattering approach.[9] Our interest is to compare two models of muffin-tin potentials for ionic materials and to see whether the choice of potential affects the oxygen K ELNES. In particular, we would like to know if the near-edge structure is sensitive to the ionicity and whether it could be used as a method to determine the charge at a particular site. These three oxides have the same sodium chloride structure, and the lattice constants for MgO, CaO, and SrO are 4.21, 4.81, and 5.16 Å, respectively.

Calculations for the oxygen K shell near-edge structure of NiO,[12] MgO,[13] and CaO (Ref. 15) have been published but there have been no studies of trends across a number of compounds with the same structure. A systematic study should enable us to separate those features which are related to differences in potential or interatomic distances from features due to differences in coordination. Our calculations are also a test of the one-electron theory for near-edge structure. There has been some controversy on whether it is necessary to include core-hole or other many-body effects to get agreement with experimental spectra.[11–15]

II. MUFFIN-TIN POTENTIALS

The muffin-tin approximation to the actual crystal potential has been applied to a number of calculations of electronic properties of crystals. For instance, it has been used in the augmented-plane-wave (APW) method for electronic band-structure calculation,[27] and in the calculation of low-energy electron diffraction.[28] The most widely used muffin-tin potential is the one suggested by

Mattheiss,[29] where the spherically symmetric contributions from the atomic potentials of all neighboring atoms are superposed on the atomic potential of the central atom to yield its muffin-tin potential. If the crystal is an ionic one, a Madelung electrostatic correction is also included. Since the radius of a muffin-tin sphere is arbitrary as long as the muffin-tin spheres do not overlap, the muffin-tin potential can be adjusted to best fit the experimental data by varying the muffin-tin radius. This flexibility of muffin-tin potential approximation plays an important role in its successful applications to a variety of materials. However, it is this type of flexibility that also causes uncertainty on how to choose the muffin-tin radius in the case of alloys and compounds. Also the way to treat charge transfer is left in the hands of individual users.

As a typical ionic material, MgO has been of much interest. We shall take it as an example here to study the following two common models for constructing muffin-tin potentials. There are other models used by different authors to incorporate the transition states and core-hole effects[13] and also the charge transfer.[13–16] We shall confine ourselves to ground-state potential models only.

The wave functions of various electronic configurations are calculated using the Herman-Skillman program,[30] and the local-density approximation is employed for the exchange energy. The statistical exchange parameter α used is the one obtained by Schwarz to give the lowest total atomic energy.[31]

One way to construct a muffin-tin potential is by the superposition of neutral atomic charge densities and potentials. We shall refer to this as model I. The muffin-tin radii are chosen so that the difference ΔV between the final potential on the edge of the magnesium and oxygen muffin-tin spheres is minimized. In Fig. 1, we plot ΔV as a function of the oxygen muffin-tin radius, while the magnesium muffin-tin radius is chosen such that the two spheres contact. The oxygen muffin-tin radius R_O determined in this way should be in the range of 1.7–2.1 bohr, and the magnesium muffin-tin sphere R_{Mg} is therefore 2.1–1.7 bohr. The potential along the [100] direction is plotted in Fig. 2. In our calculations, we choose $R_O = 1.8$ bohr and $R_{Mg} = 2.15$ bohr, respectively. The total charge densities $4\pi\rho(r)r^2$ are also plotted as a function of radial distance r, as shown in Fig. 3.

The effect of charge transfer from oxygen to magnesium is expected to be partly achieved through the fact that the magnesium $3s$ wave function is less localized around the atomic site, and some portion of it will fall into the muffin-tin sphere of the neighboring oxygen site. The charge density $4\pi\rho(r)r^2$ of neutral magnesium $3s$ peaks at 2.7 bohr. Using the muffin-tin radii given above, we found that the contribution from the superposition of wave functions of all neighboring atoms increases the total number of electrons inside each oxygen muffin-tin sphere from its atomic value of 6.86 electrons to 7.24 electrons, an increase of 0.38 electrons. This is only about 20% of the expected two-electron charge transfer. At the same time, the total number of electrons inside each magnesium muffin-tin sphere increases from its atomic value of 10.33 electrons to 10.92 electrons, an increase of 0.59 electrons. There are 1.84 electrons in the space between muffin-tin spheres. Since the spherically symmetric contribution from neighboring atoms is always a positive charge-density term, we expect the total number of electrons inside both the oxygen and magnesium muffin-tin spheres to be larger than their atomic values. We conclude that for the above muffin-tin radii the effect of charge transfer cannot be achieved by superposition of wave functions. At the largest oxygen muffin radius, $R_O = \frac{1}{2}a_0/\sqrt{2} = 2.80$ bohr, there are 9.58 electrons inside the oxygen muffin-tin sphere and 9.35 electron inside the magnesium sphere.

The second way to construct the muffin-tin potential

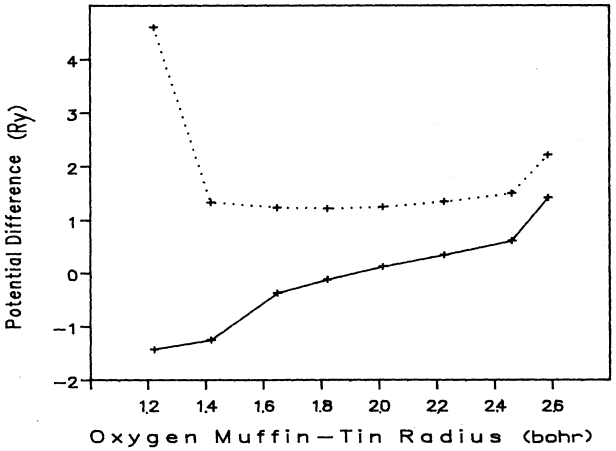

FIG. 1. The potential difference at the oxygen and magnesium muffin-tin sphere (in Ry) as a function of oxygen muffin-tin radius. The solid line is for model I, and the dotted line is for model II.

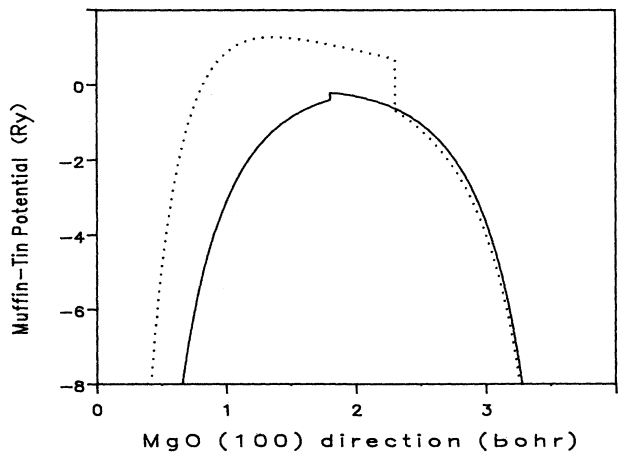

FIG. 2. The muffin-tin potential along MgO(100) direction, O-Mg distance is 3.97 bohr. The solid line is for model I and the dotted line is for model II.

begins with Mg^{2+} and O^{2-} ionic potentials. We shall refer to this as model II. As O^{2-} is unstable as a free anion but is found to be stable in crystal environment, the Watson sphere technique[32] has been employed to obtain O^{2-} wave functions. The O^{2-} anion is contained inside a Watson sphere at radius R_W with uniformly-distributed positive charge $Q_W=+2e$. The parameters associated with the Watson sphere are the total charge Q_W, which equals to the ionicity of the anion, and the Watson radius R_W. For the case of O^{2-} anion, R_W is of the range of 1.2–1.4 Å. The parameters for muffin-tin potentials of MgO and CaO of this model are the same as these used by Redinger and Schwarz in their APW electronic band-structure calculations,[33] $R_O=2.299$ and $R_{Mg}=1.679$ bohr. The total number of electrons inside the oxygen and magnesium muffin-tin spheres are 9.58 and 9.92 electrons, respectively. There is only 0.5 electron in the space between muffin-tin spheres. Also it is noted that the difference between the potentials at the oxygen and magnesium muffin-tin spheres is greater than 1.2 Ry and remains almost the same over a larger range of muffin-tin radii. This is because the potential at the muffin-tin sphere of O^{2-} is not much different from that of neutral oxygen, but the potential at the muffin-tin sphere of Mg^{2+} is much lower than that of neutral Mg.

We compare the total charge densities for these two models in Fig. 3. The difference in magnesium total charge density is insignificant for radial distances r less than 1.5 bohr, and is only apparent for r greater than 1.5 bohr, as the wave functions of $1s^2 2s^2 2p^6$ orbitals of Mg and Mg^{2+} are almost identical. We would also expect the magnesium muffin-tin potentials to be almost the same, as shown in Fig. 2. However, the difference between the total oxygen charge density for these two models is more significant, and there are large differences for radial distances greater than 0.5 bohr. Therefore, we expect the muffin-tin potential for oxygen of these two models to be quite different beginning at radial distances r greater than 0.5 bohr. In Fig. 4, we plot the integrated total charge inside radius r,

$$q(r)=\int_0^r 4\pi\rho(r')r'^2dr' \ . \tag{1}$$

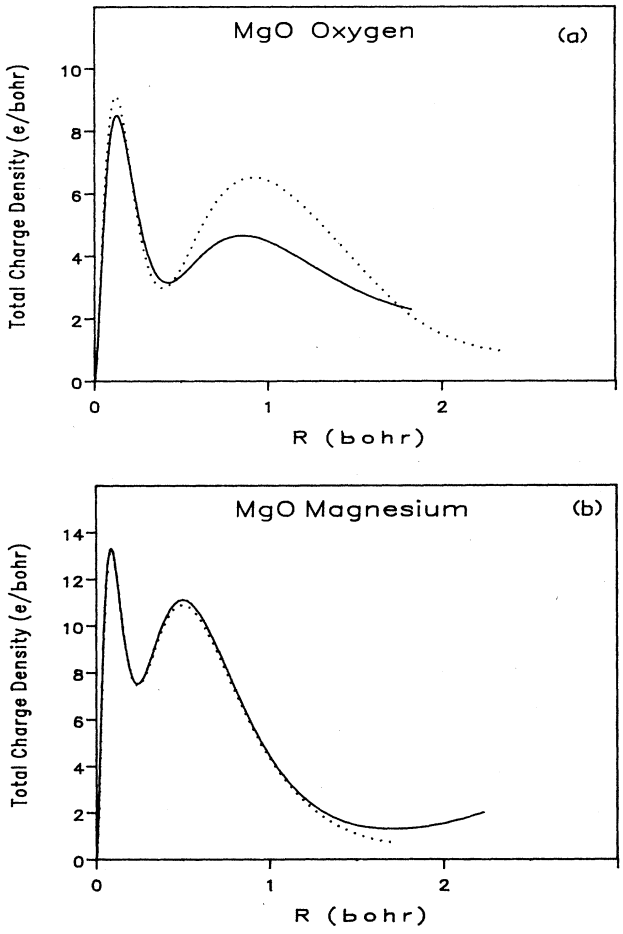

FIG. 3. The total electron charge densities inside the muffin-tin spheres of (a) oxygen and (b) magnesium for model I (solid line) and model II (dotted line).

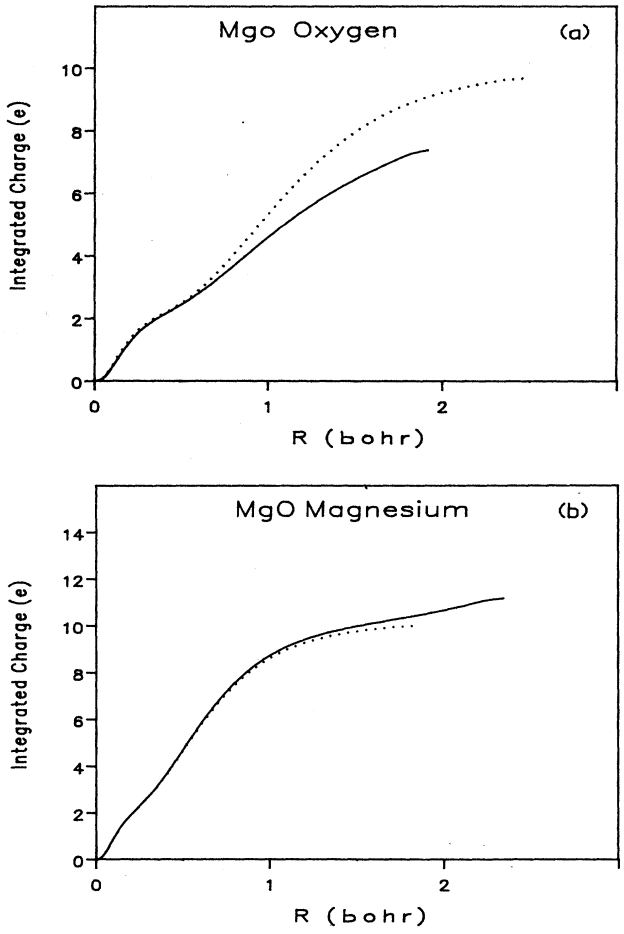

FIG. 4. The integrated charge $q(r)$ for (a) oxygen and (b) magnesium in units of an electron.

The difference in muffin-tin potentials will result in a difference in the phase shifts based on these potentials. The phase shifts of both oxygen and magnesium for the two muffin-tin potential models are listed in Table I, where KE is the kinetic energy of the ejected electron. To make the comparison easier, a constant π is added to the s and p phase shifts of oxygen calculated from model II. As we can see, the magnesium phase-shifts for the two models are very close to each other, whereas the oxygen phase shafts show greater differences. This would be expected from the differences in muffin-tin potentials.

The scattering of electrons of energy E by the atom is given by the usual partial wave expansion,

$$t_l(E)=\sin\delta_l(E)e^{i\delta_l(E)}, \tag{2}$$

where $\delta_l(E)$ is the phase shift for angular momentum l.

III. OXYGEN K ELNES

To calculate the near-edge structure, the scattering from shells of atoms around the ionized atom is first calculated and then the overall reflected wave at the ionized

TABLE I. Phase-shifts of oxygen and magnesium of MgO (unit: radius).

KE	Model I				Model II			
(eV)	s	p	d	f	s	p	d	f
				Oxygen				
2	5.650	2.894	0.000	0.000	5.783	3.099	−0.001	0.000
4	5.412	2.776	0.002	0.000	5.585	3.039	−0.006	0.000
6	5.241	2.690	0.004	0.000	5.440	2.975	−0.015	−0.001
8	5.106	2.621	0.009	0.000	5.323	2.913	−0.028	−0.002
10	4.993	2.563	0.015	0.000	5.225	2.854	−0.044	−0.003
12	4.897	2.512	0.023	0.001	5.143	2.798	−0.062	−0.006
14	4.812	2.467	0.033	0.001	5.072	2.746	−0.083	−0.009
16	4.737	2.428	0.045	0.002	5.012	2.698	−0.105	−0.013
18	4.670	2.392	0.059	0.003	4.962	2.653	−0.129	−0.018
20	4.609	2.360	0.075	0.004	4.920	2.613	−0.153	−0.024
22	4.553	2.331	0.093	0.005	4.886	2.577	−0.177	−0.032
24	4.501	2.304	0.113	0.006	4.860	2.545	−0.202	−0.040
26	4.454	2.280	0.135	0.008	4.841	2.518	−0.227	−0.048
28	4.410	2.258	0.158	0.010	4.829	2.495	−0.251	−0.058
30	4.369	2.238	0.183	0.012	4.824	2.476	−0.275	−0.068
32	4.331	2.220	0.208	0.015	4.825	2.463	−0.298	−0.079
34	4.295	2.203	0.235	0.018	4.831	2.454	−0.321	−0.091
36	4.261	2.187	0.262	0.021	4.842	2.449	−0.343	−0.102
38	4.229	2.173	0.290	0.025	4.856	2.451	−0.364	−0.115
40	4.199	2.160	0.319	0.029	4.874	2.457	−0.384	−0.127
42	4.170	2.148	0.347	0.033	4.895	2.468	−0.402	−0.140
44	4.143	2.137	0.375	0.038	4.916	2.484	−0.420	−0.153
				Magnesium				
2	6.135	3.143	0.001	0.000	6.039	3.134	0.000	0.000
4	6.060	3.146	0.004	0.000	5.942	3.124	0.002	0.000
6	5.996	3.150	0.011	0.000	5.870	3.113	0.006	0.000
8	5.937	3.154	0.023	0.001	5.811	3.103	0.011	0.000
10	5.881	3.157	0.038	0.001	5.759	3.095	0.020	0.000
12	5.828	3.159	0.058	0.003	5.714	3.088	0.031	0.001
14	5.778	3.160	0.082	0.004	5.672	3.082	0.044	0.001
16	5.730	3.159	0.110	0.006	5.634	3.077	0.061	0.002
18	5.683	3.157	0.141	0.009	5.598	3.073	0.082	0.003
20	5.639	3.153	0.176	0.012	5.564	3.070	0.105	0.004
22	5.595	3.148	0.214	0.017	5.532	3.067	0.132	0.005
24	5.554	3.141	0.253	0.021	5.502	3.065	0.163	0.007
26	5.514	3.133	0.294	0.027	5.472	3.063	0.196	0.009
28	5.475	3.124	0.335	0.033	5.444	3.061	0.233	0.011
30	5.437	3.115	0.376	0.040	5.416	3.059	0.273	0.014
32	5.401	3.104	0.417	0.047	5.390	3.057	0.314	0.017
34	5.366	3.093	0.456	0.055	5.364	3.055	0.358	0.020
36	5.332	3.081	0.493	0.064	5.338	3.052	0.403	0.024
38	5.299	3.069	0.529	0.073	5.313	3.049	0.449	0.029
40	5.267	3.057	0.563	0.083	5.289	3.046	0.495	0.033
42	5.237	3.044	0.594	0.094	5.265	3.043	0.541	0.039
44	5.207	3.031	0.623	0.104	5.242	3.039	0.585	0.044

atom is obtained by considering the scattering between shells. We used the computer code of Durham, Pendry, and Hodges.[9] Although this program is intended for x-ray absorption near-edge structure (XANES), it is applicable to ELNES for small angles where the momentum change is small and dipole transitions dominate.

The other factors that affect the calculation of near-edge structure include the attenuation due to inelastic scattering processes and the number of shells of neighboring atoms in the cluster. The inelastic attenuation is simulated with an imaginary part of the potential, either an energy-independent value of the order of $V_i = 1$ eV or an energy-dependent value determined from a mean free path of about 5–10 Å. The number of shells in the calculation is affected by the neighboring site positions, the scattering amplitudes at these sites and the attenuation, and can be determined by a convergence test. The greater the inelastic attenuation and the smaller the scattering amplitude, the fewer shells of neighboring atoms that are required. In the present work, we used a cluster of 6 to 10 shells, or 84 to 174 atoms.

The electron-energy-loss spectra of CaO and SrO were recorded on a Philips 400T electron microscope equipped with a Gatan 607 sequential electron-energy-loss spectrometer and a Tracor Northern 2000 multichannel analyzer. The powder-crystalline specimen were of a dimension of 100–1000 Å. The plural scattering contribution, which is due to the incident electrons experiencing inelastic scattering processes more than once, can be reduced by acquiring an EEL spectrum from an area thin enough in comparison with the total inelastic mean free path λ. This can be easily checked through the low loss region of an EEL spectrum. Electron diffraction patterns were monitored to avoid detectable structural and compositional changes of the specimen under the illumination of the electron beam.

The experimental conditions were as follows. The accelerating voltage was 120 keV and the incident beam was collimated to 6.8 mrad. The spectrometer collected electrons scattered up to 7.1 mrad, which gives a maximum $\mathbf{q}$ vector of 0.21 Å^{-1}. The spectra were recorded at 0.1 eV per channel with a recording time of 0.5 to 1 sec for each channel. The pre-edge background was subtracted by fitting the usual empirical inverse power law,[1,2] AE^{-r}, where A and r are constants and E is the energy loss. The MgO spectrum was recorded on an HB501 scanning transmission electron microscope by T. Manoubi and C. Colliex at Laboratoir de Physique des Solides, Orsay, France. The accelerating voltage was 100 keV and the incident angle was 15 mrad; the collection angle was 25 mrad, giving a maximum $\mathbf{q}$ of 0.67 Å^{-1}. This spectrum was recorded at 0.1 eV per channel with a time interval of 0.14 sec per channel. The spectrum is processed in the same way as the other oxide spectra.

A. MgO

The oxygen K near-edge structure (O-K NES) of MgO was calculated using the two muffin-tin potential models. The results are shown in Fig. 5. Both models give three peaks, corresponding to the first three peaks in the EEL spectrum. We found that the O-K NES based on these two muffin-tin models are essentially the same, although the peak positions from model I are closer to the experimental spectra than those from model II. Our present result is comparable with the oxygen K NES of Lindner *et al.*,[13] who used a similar muffin-tin potential to model I except that the potential of the central oxygen atom was replaced by that of a free fluorine atom as suggested by the $Z+1$ approximation to take account of the core-hole effect. Our result gives a better agreement with experiment for peak positions than the result of Lindner *et al.*, which also shows a splitting at the first peak. By varying the oxygen muffin-tin radius from 1.75–2.0 bohr, we observed very little change in the near-edge structures.

B. CaO

The above methods for constructing the muffin-tin potentials of MgO can be applied to CaO. For the muffin-tin potential model I, we found the muffin-tin radius of

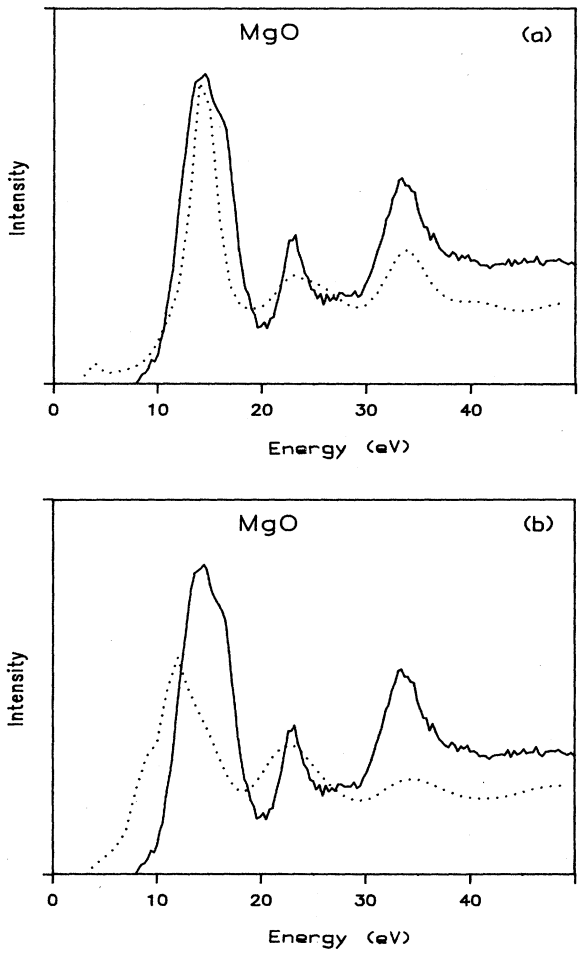

FIG. 5. The oxygen K near-edge structures of MgO calculated using muffin-tin potentials of (a) model I and (b) model II are shown as the dotted lines. The solid lines are the experimental EEL spectrum (Colliex and Manoubi).

oxygen should be 1.9–2.3 bohr and that of calcium should be 2.25–2.65 bohr. In the present calculation, we use $R_O = 2.0$ and $R_{Ca} = 2.55$ bohr. There are 7.53 electrons inside the oxygen muffin-tin sphere, and 18.6 electrons inside the calcium one, with 1.87 electrons in the space between the muffin tins. For this set of muffin-tin radii, we again realize that the effect of charge transfer cannot be achieved by the superposition of charge densities. For the muffin-tin potential model II, the muffin-tin radii of O^{2-} and Ca^{2+} are 2.336 and 2.216 bohr. The Watson sphere for O^{2-} is at $R_W = 2.5946$ bohr. There are 9.24 electrons inside the O^{2-} muffin-tin sphere, 17.7 electrons inside of that of Ca^{2+}, and 1.06 electrons in the space between all muffin tins. Again, we found that there are more electrons included inside muffin-tin spheres in model II than in model I.

The oxygen K near-edge structures of CaO calculated using these two models of muffin-tin potentials are shown in Fig. 6. The same number of major peaks are present in both calculations, which are in good agreement with the experimental ELNES. We found with the parameters given above, the muffin-tin potential model II gives a result comparable to that of model I, although the results from muffin-tin potential model I is in slightly better agreement with experiment. The first major peak for model II is shifted closer to the threshold than that of model I, whereas the other major peaks occur at almost the same energies. Our work is in agreement with a similar calculation of oxygen K NES of CaO by Willie *et al.*,[15] who used a point charge model to simulate possible charge transfer.

C. SrO

The muffin-tin potential of SrO is constructed using the following set of muffin-tin radii for oxygen and strontium, $R_O = 2.0$ bohr and $R_{Sr} = 2.87$ bohr. We found there are 7.48 electrons inside the oxygen muffin-tin sphere and

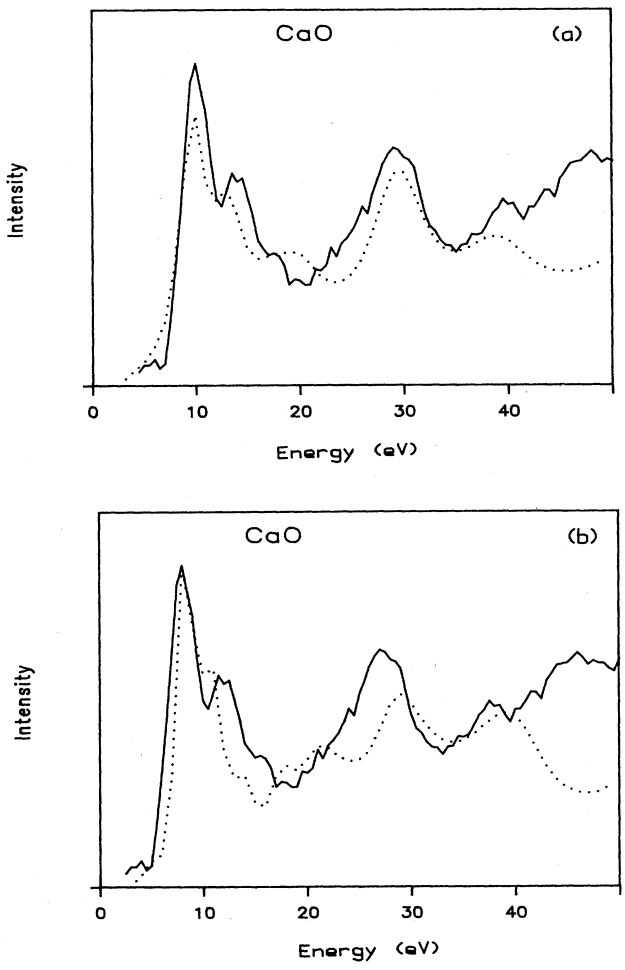

FIG. 6. The oxygen K near-edge structures of CaO calculated using muffin-tin potentials of (a) model I and (b) model II are shown as the dotted lines. The solid lines are the experimental EEL spectrum.

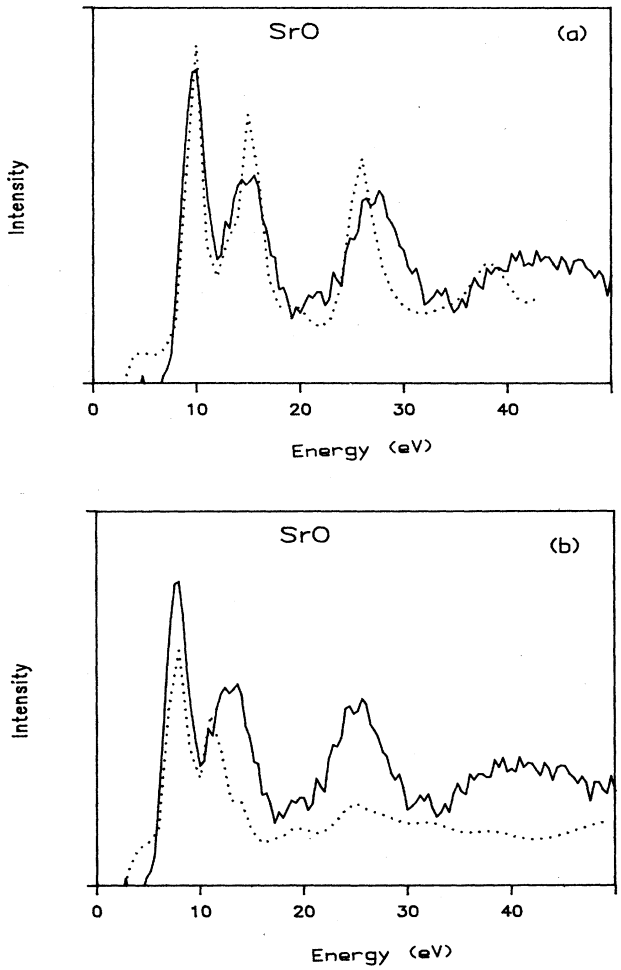

FIG. 7. The oxygen K near-edge structures of SrO calculated using muffin-tin potentials of (a) model I and (b) model II are shown as the dotted lines. The solid lines are the experimental EEL spectrum.

36.80 electrons inside the strontium sphere, the other 1.72 electrons are outside the muffin-tin spheres. Since there is no APW band calculation for SrO which also gives the best fit for a Watson radius R_W, we use the same value for the O^{2-} radius as we used for CaO. The muffin-tin radii for oxygen and strontium are $R_O = 2.36$ bohr and $R_{Sr} = 2.51$ bohr. There are 9.59 electrons inside the oxygen muffin-tin sphere, 35.56 electrons inside the strontium muffin-tin sphere, and 0.85 electrons outside the muffin-tin spheres. As in the case of both MgO and CaO, we found there are more electrons inside the muffin-tin spheres in model II than in model I.

The calculated oxygen K near-edge structures using these two models are shown in Fig. 7. As far as the first peak is concerned, the calculation based on model I is in better agreement with experiment than that based on model II. The differences between the two calculations are not great, though there are more peaks in the calculation using model II and the major peaks are shifted closer to the threshold.

IV. CONCLUSIONS

For an oxygen muffin-tin radius R_O in the range of 1.8–2.3 bohr, the effect of charge transfer cannot be achieved by superposition of charge densities. If the largest possible R_O is used, the total number of electrons inside the oxygen muffin-tin sphere could approach the ten electrons of O^{2-} anion. The muffin-tin potential based on ionic potentials usually has more electrons inside the muffin-tin spheres, and consequently has fewer electrons in the space outside the muffin tins. Changing the oxygen muffin-tin radius in the range of 1.8–2.3 bohr does not result in appreciable changes in the calculated near-edge structures.

In the case of oxygen K near-edge structure of MgO, CaO, and SrO, both the muffin-tin potential models I and II give results in reasonable agreement with the EEL spectrum. It appears that the calculations based on model I using neutral atoms are closer to the experimental results in both peak heights and peak positions than the model II calculations based on ionized atoms. Our results lead us to the possibility that we might find more than one form of muffin-tin potentials yielding reasonable near-edge structures, although their potentials and phase shifts are noticeably different. If this is the case, we will not be able to determine uniquely the charge transfer from the near-edge spectrum. In other words, our results seem to suggest that the near-edge fine structure is more sensitive to the coordination of neighboring atoms, and is less sensitive to possible charge transfers between atoms.

We also found the ground-state muffin-tin potential is adequate for the calculation of the oxygen K near-edge structures. As it appears that different potentials can give spectra in reasonable agreement with experiment, it would seem that it is questionable to assume that features in near-edge spectroscopy provide unambiguous evidence for core-hole or other many-body effects.

ACKNOWLEDGMENTS

We are grateful to Dr. C. Colliex and Dr. T. Manoubi for providing us the MgO O-K EEL spectrum. Financial support from Arizona State University and the facility for high-resolution electron microscopy (HREM) (National Science Foundation Grant No. DMR-8611609) is also acknowledged.

[1]R. F. Egerton, *Electron Energy Loss Spectroscopy in the Electron Microscope* (Plenum, New York, 1986).
[2]C. Colliex, in *Advances in Optical and Electron Microscopy,* edited by V. E. Cosslett and R. Barer (Academic, London, 1984), Vol. 9, p. 65.
[3]M. S. Issacson and D. Johnson, Ultramicroscopy **1**, 33 (1975).
[4]R. F. Egerton, Ultramicroscopy **3**, 243 (1978).
[5]R. D. Leapman, P. Rez, and D. F. Mayers, J. Chem. Phys. **72**, 1232 (1980).
[6]C. Colliex and B. Jouffrey, Philos. Mag. **25**, 491 (1972).
[7]A. E. Meixner, M. Schlüter, P. M. Platzman, and G. S. Brown, Phys. Rev. B **17**, 686 (1978).
[8]L. A. Grunes, R. D. Leapman, C. Wilker, R. Hoffmann, and A. B. Kunz, Phys. Rev. B **25**, 7157 (1982).
[9]P. J. Durham, J. B. Pendry, and C. H. Hodges, Comput. Phys. Commun. **25**, 193 (1982).
[10]F. Sette, J. Stöhr, and A. P. Hitchcock, J. Chem. Phys. **81**, 4096 (1984).
[11]D. Norman, K. B. Garg, and P. J. Durham, Solid State Commun. **56**, 895 (1985).
[12]D. D. Vvedensky and J. B. Pendry, Surf. Sci. **152/153**, 33 (1985).
[13]Th. Lindner, H. Sauer, W. Engel, and K. Kambe, Phys. Rev. B **33**, 22 (1986).
[14]M. M. Disko, J. C. H. Spence, O. F. Sankey, and D. K. Saldin, Phys. Rev. B **33**, 5642 (1986).
[15]L. T. Willie, P. J. Durham, and P. A. Sterne, J. Phys. (Paris) Colloq. **47**, C8-43 (1986).
[16]X. Weng and P. Rez, Ultramicroscopy **25**, 345 (1988).
[17]S. Csillag, D. E. Johnson, and E. A. Stern, in *EXAFS in Material Science,* edited by B. K. Teo and D. C. Joy (Plenum, New York, 1981).
[18]M. M. Disko, O. L. Krivanek, and P. Rez, Phys. Rev. B **25**, 4252 (1982).
[19]D. E. Sayers, E. A. Stern, and F. W. Lytle, Phys. Rev. Lett. **27**, 1204 (1971).
[20]C. A. Ashley and S. Doniach, Phys. Rev. B **11**, 1279 (1975).
[21]P. A. Lee and J. B. Pendry, Phys. Rev. B **11**, 2795 (1975).
[22]J. J. Rehr, E. A. Stern, R. L. Martin, and E. R. Davidson, Phys. Rev. B **17**, 560 (1978).
[23]A. Bianconi, M. Dell'Ariccia, A. Gargano, and C. R. Natoli, in *EXAFS and Near Edge Structure,* edited by A. Bianconi, L. Incoccia, and S. Stipcich (Springer-Verlag, New York, 1982), p. 57.
[24]J. E. Müller and W. L. Schaich, Phys. Rev. B **27**, 6489 (1983).
[25]M. Kitamura, C. Sugiura, and S. Muramatsu, Solid State Commun. **62**, 663 (1987).
[26]P. E. Batson, K. L. Kavanagh, C. Y. Wong, and J. M. Wood-

all, Ultramicroscopy **22**, 89 (1987).
[27]T. L. Loucks, *Augmented Plane Wave Method* (Benjamin, New York, 1967).
[28]J. B. Pendry, *Low Energy Electron Diffraction* (Academic, London, 1974).
[29]L. F. Mattheiss, Phys. Rev. **134**, A970 (1964).
[30]F. Herman and S. Skillman, *Atomic Structure Calculations* (Prentice-Hall, Englewood Cliffs, New Jersey, 1963).
[31]K. Schwarz, Phys. Rev. B **5**, 2466 (1972).
[32]R. E. Watson, Phys. Rev. **111**, 1108 (1958).
[33]J. Redinger and K. Schwarz, Z. Phys. B **40**, 269 (1981).